Chapter 9

Non-additive kinetic energy and potential in analytically solvable systems and their approximated counterparts

Tomasz A. Wesolowski[1] and Andreas Savin[2]

[1]*Department of Physical Chemistry, University of Geneva, 30, quai Ernest-Ansermet, CH-1211 Geneva 4, Switzerland*
tomasz.wesolowski@unige.ch

[2]*Laboratoire de Chimie Theorique, CNRS and Universite Pierre et Marie Curie (Paris VI), Paris, France*
andreas.savin@lct.jussieu.fr

The one-electron equation for orbitals embedded in frozen electron density (Eqs. 20-21 in [Wesolowski and Warshel, *J. Phys. Chem*, **97** (1993) 8050]) in its exact and approximated version is solved for an analytically solvable model system. The system is used to discuss the role of the embedding potential in preventing the collapse of a variationally obtained electron density onto the nucleus in the case when the frozen density is chosen to be that of the innermost shell. The approximated potential obtained from the second-order gradient expansion for the kinetic energy prevents such a collapse almost perfectly but this results from partial compensation of flaws of its components. It is also shown that that the quality of a semi-local approximation to the kinetic-energy functional, a quantity needed in orbital-free methods, is not related to the quality of the non-additive kinetic energy potential - a key component of the effective embedding potential in one-electron equations for embedded orbitals.

Contents

9.1. Introduction

The basic formal results of Frozen-Density Embedding Theory (FDET), which is of the greatest relevance to any multi-level computational methods, is the fact that minimization of the Hohenberg-Kohn energy functional ($E^{HK}[n]$) in the presence of the constraint $n \geq n_B$, where n_B is some given in advance (frozen) electron density,

can be achieved by means of a suitably chosen *embedding potential*, i.e., a multiplicative (local) operator. Moreover, the non-electrostatic component of this potential is the bi-functional depending on n_B and n_A, where n_A is the embedded electron density, i.e., the density which is to be optimized.[1,9,10,19] According to FDET, the exact embedding potential comprises a component which is the functional derivative of the bi-functional of the non-additive kinetic energy ($T_s^{nad}[n_A, n_B]$). This component is the greatest relevance for the present volume. In principle, any approximation for the kinetic energy functional $T_s[n]$ used in OF-DFT can be trivially used to approximate also $T_s^{nad}[n_A, n_B]$ (see Eq. 9.1.5 below). Our numerical experience indicates, however, that the quality of any given approximation to $T_s[n]$ is not correlated with that of the resulting approximation for $T_s^{nad}[n_A, n_B]$.[4,20] Turning back to FDET, its formal framework provides the basis for a large variety of computational methods aiming at quantitative predictions of the effect of environment on electronic structure of embedded species (see Ref.[3] or articles reviewed in chapters 10 and 11 in the present volume, for instance). The key steps resulting in the development of FDET-based computational methods and ther practical applications include: *i*) Introduction of the GGA97 approximation[5] for the bi-functional of the non-additive kinetic potential and energy. The GGA97 approximation to $T_s^{nad}[n_A, n_B]$ eliminates to large extend the spurious component of the non-additive kinetic potential occurring if this potential is obtained from the gradient expansion of $T_s[n]$.[4] *ii*) Development of the gradient-expansion-approximation based approximation for $T_s^{nad}[n_A, n_B]$ (NDSD), which enforces one of the exact properties of the bi-functional $v_t^{nad}[n_A, n_B]$ leading to an improvement of the embedding potential near the nuclei in the environment.[6] *iii*) Combining the ground-state FDET with the linear-response time-dependent DFT strategy for electronic excitations[7,8]. *iv*) The proof that the original orbital-free effective embedding potential derived for embedding a reference system of non-interacting electrons is also the optimal effective embedding potential for embedding interacting systems[9] or systems described by means of first-order density matrix.[10] These developments were matched by the improvements of the numerical implementation as well as techniques to generate the frozen electron density. Currently, the ADF code[12] provides the most advanced and flexible implementation of FDET based methods. This implementation was made by Wesolowski (see for instance Refs.[8]) and subsequently developed by others. For the most recent implementations, see Ref.[2,3] Several refinements and further advancements in both numerical implementation as well as in the theory of embedding such as an efficient method to account for dynamic response of the environment in evaluation of electronic excited levels (see chapter 11 of this volume) or explicit corrections for erroneous behavior of the embedding potential at dissociation,[23] for instance, expanded the domain of applicability of the orbital-free embedding potential. Unfortunately, similarly to Kohn-Sham and orbital-free DFT formulation, the computational methods based on FDET suffer from the fact that they rely on approximations for the needed density functionals and only in a few cases the an-

alytical expresions for quantities defined in FDET are available.[6,22,23] The present chapter intends to fill the gap. We analyze in detail an analytically solvable case where *all* quantities defined in FDET can be evaluated analytically and compared with approximated quantities needed in practical simulations.

The key object in FDET is the orbital-free embedding potential which depends on the quantum mechanical descriptor used for n_A in order to optimize it. In the case of embedding a non-interacting reference system, one-particle reduced density matrix, and interacting wavefunction of the full Configuration Interaction form, this potential reads (see for instance Eq. 3 in Ref.[11]):

$$v^{emb}_{KSCED}[n_A, n_B, v^B_{ext}](\vec{r}) = v^B_{ext}(\vec{r}) + \int \frac{n_B(\vec{r}')}{|\vec{r}' - \vec{r}|} d\vec{r}' + \tag{9.1.1}$$
$$\left.\frac{\delta E_{xc}[n]}{\delta n(\vec{r})}\right|_{n(\vec{r})=n_A(\vec{r})+n_B(\vec{r})} - \left.\frac{\delta E_{xc}[n]}{\delta n(\vec{r})}\right|_{n(\vec{r})=n_A(\vec{r})} +$$
$$\left.\frac{\delta T_s[n]}{\delta n(\vec{r})}\right|_{n(\vec{r})=n_A(\vec{r})+n_B(\vec{r})} - \left.\frac{\delta T_s[n]}{\delta n(\vec{r})}\right|_{n(\vec{r})=n_A(\vec{r})} ,$$

where the functionals $E_{xc}[n]$ and $T_s[n]$, are defined as in Kohn-Sham formulation of Density Functional Theory.[13] In the present considerations and in practical applications of Eq. 9.1.1, opposite to methods based on the Kohn-Sham theory, the functional $T_s[n]$ is considered as a density functional defined in the Levy-Lieb constrained search formulation[14,15] because the Kohn-Sham orbitals are not available for the *total* electron density.

Eq. 9.1.1 shows clearly that explicit quantum mechanical descriptors - such orbitals - do not have to be known for the environment. Instead, the electron- ($n_B(\vec{r})$) and nuclear charge density only provide sufficient information to generate the embedding potential for any given $n_A(\vec{r})$. For this reason, we refer to the potential defined in Eq. 9.1.1 as the *orbital-free embedding potential*. This correspondence provides the basis for various computational methods for multi-level simulations, such as the ones reviewed in Chapters 10 and 11, but constructing in practice the potential defined in Eq. 9.1.1 represents the main challenge for the .[1,9,10,19]

If the embedded system is described by means of a reference system of non-interacting electrons, $n_A(\vec{r})$ is constructed from embedded orbitals (φ_i):

$$n_A(\vec{r}) = \sum_i^{Nocc} 2|\varphi_i|^2 , \tag{9.1.2}$$

which are obtained from one-electron equations for embedded orbitals (Eqs. 20-21

in Ref.[1]):

$$\left[-\frac{1}{2}\nabla^2 + v^A_{ext}(\vec{r}) + \int \frac{n_A(\vec{r}')}{|\vec{r}' - \vec{r}|} d\vec{r}' + v_{xc}[n_A](\vec{r}) + v^{emb}_{KSCED}[n_A, n_B, v^B_{ext}](\vec{r})\right] \varphi^A_i = \epsilon_i \varphi^A_i \tag{9.1.3}$$

For the sake of simplicity, equations are given for spin-compensated electron densities: hence the factor 2 in Eq. 9.1.2. The acronym KSCED in Eqs.9.1.1 and 9.1.3 stands for the Kohn-Sham Equations with Constrained Electron Density and is used to distinguish the effective potential and the orbitals in Eq. 9.1.3 from their counterparts in the Kohn-Sham equations.

Eq. 9.1.1 shows clearly that, except for $v^B_{ext}(\vec{r})$, the position dependency of each other term in $v^{emb}_{KSCED}[n_A, n_B, v^B_{ext}](\vec{r})$ is determined by the position dependency of $n_A(\vec{r})$ and $n_B(\vec{r})$. These components of the potential are, therefore, functionals of these two densities. In particular, the kinetic-energy functional dependent component of the potential given in Eq. 9.1.1, for which the following short notation will be used:

$$v^{nad}_t[n_A, n_B] = \left.\frac{\delta T_s\,[n]}{\delta n(\vec{r})}\right|_{n(\vec{r})=n_A(\vec{r})+n_B(\vec{r})} - \left.\frac{\delta T_s\,[n]}{\delta n(\vec{r})}\right|_{n(\vec{r})=n_A(\vec{r})} \tag{9.1.4}$$

is also a functional $n_A(\vec{r})$ and $n_B(\vec{r})$. The symbol, $v^{nad}_t[n_A, n_B]$, which denotes the correspondence between the densities $n_A(\vec{r})$ and $n_B(\vec{r})$ should be distinguished from $v_t(\vec{r})$. Although $v_t(\vec{r})$ is uniquely determined by the $v^{nad}_t[n_A, n_B]$, knowing $v^{nad}_t(\vec{r})$ does not imply that the corresponding $v^{nad}_t[n_A, n_B]$ is known. This distinction is reflected in the notation applied in the present work for any other local quantities (potentials) which are defined as density functionals or bi-functionals. For instance, $v[n]$ denotes a functional i.e., the correspondence between a function $n(vecr$ and another function (potential for instance) $v(\vec{r})$ whereas $v[n](\vec{r})$ denotes a function evaluated at for some $n(\vec{r})$.

The potential given in Eq. 9.1.4 is not only the component of the effective potential in Eq. 9.1.3, i.e., the case where the embedded system is described by means of the reference system of non-interacting electrons. It is also the component of the exact embedding potential in cases were the embedded density $n_A(\vec{r})$ is obtained in other methods based on variational principle, in which the electron-electron interactions are treated as: *i*) the expectation value of the exact Hamiltonian calculated over a class of trial wavefunctions of the form ranging from Hartree-Fock- to full CI wavefunction[9] or *ii*) a functional depending on one-particle density matrix.[10] ,

Multiconfigurational Self-Consistent Field (MSCF) or Configuration Interaction (CI) methods, the correspondence between the embedding potential and the pair of densities $n_A(\vec{r})$ and $n_B(\vec{r})$ depends In view of the practical applications of the outlined embedding formalism, it is convenient to introduce the bi-functional of the non-additive kinetic energy:

$$T^{nad}_s[n_A, n_B] = T_s[n_A + n_B] - T_s[n_A] - T_s[n_B] \tag{9.1.5}$$

The bi-functional $T_s^{nad}[n_A, n_B]$ represent one of the components of the total energy of the system, whereas its functional derivative with respect to $n_A(\vec{r})$ is $v_t^{nad}(\vec{r})$ which can be expressed alternatively as:

$$v_t^{nad}[n_A, n_B] = \left. \frac{\delta T_s^{nad}[n, n_B]}{\delta n(\vec{r})} \right|_{n(\vec{r})=n_A(\vec{r})} \tag{9.1.6}$$

In practical applications of Eq. 9.1.3, $v_t^{nad}[n_A, n_B]$ needs to be approximated by means of some approximation depending explicitly on the pair of electron densities $n_A(\vec{r})$ and $n_B(\vec{r})$ (approximations are denoted with tildes in the present work).

$$v_t^{nad}[n_A, n_B] \approx \tilde{v}_t^{nad}[n_A, n_B] \tag{9.1.7}$$

The above approximation leads to errors in the effective potential and consequently to the deviation between the electron density obtained from Eq. 9.1.3 and the target density $n_o(\vec{r}) - n_B(\vec{r})$). Using such density in the evaluation of the total energy leads also to errors which add to the errors due to the approximation to $T_s^{nad}[n_A, n_B]$. It is worthwhile to underline here that the quality of the results is not directly correlated with the quality of the used $\tilde{T}_s[n]$ and $\frac{\delta \tilde{T}_s[n]}{\delta n(\vec{r})}$, as it is the case of the OF-DFT methods discussed in the present volume, but rather on the quality of the differences of these quantities.

Various methodologies based on the correspondence between the pair of electron densities and the embedding potential given in Eq. 9.1.1, which use an inexpensively calculated approximation for $\tilde{v}_t^{nad}[n_A, n_B]$, were recently developed and applied in numerical simulations of condensed matter (see Refs.[16–19] and chapters 10 and 11 of this volume). An obvious strategy is to use some approximation for $T_s[n]$ and to obtain the corresponding $v_t^{nad}[n_A, n_B]$ from Eq. 9.1.4. It is convenient to call such approximations for $T_s^{nad}[n_A, n_B]$ - decomposable. Unfortunately, one cannot count on the fortuitious cancellation of errors for the potential $v_t[n]$ l calculated at different electron densities. Our previous dedicated studies[4,20] and recent comprehensive benchmarking studies reportes in Ref.[21] indicate, however, that improvements in approximating $T_s[n]$ do not necessarily lead to improvements in $v_t^{nad}[n_A, n_B]$. *Therefore, one should rather consider the quest for an usable approximation for each of the two potentials, $v_t^{nad}[n_A, n_B]$ and $v_t[n]$, to represent independent tasks.* The following strategies to approximate $v_t^{nad}[n_A, n_B]$ are, in principle, possible:

- **Decomposable approximations.**
  For any approximation $\tilde{T}_s[n]$, for which the analytical expression for its functional derivative ($\frac{\delta \tilde{T}_s[n]}{\delta n(\vec{r})}$) is known, the corresponding $\tilde{v}_t^{nad}[n_A, n_B]$ can be obtained in a straightforward manner as the difference of two analytic expressions:

  $$v_t^{nad}[n_A, n_B] \approx \tilde{v}_t^{nad}[n_A, n_B] = \left. \frac{\delta \tilde{T}_s[n]}{\delta n(\vec{r})} \right|_{n(\vec{r})=n_A(\vec{r})+n_B(\vec{r})} - \left. \frac{\delta \tilde{T}_s[n]}{\delta n(\vec{r})} \right|_{n(\vec{r})=n_A(\vec{r})} \tag{9.1.8}$$

  This is the most commonly used strategy in the literature all quantities derivable from a given approximation for $T_s[n]$ are numerically available.

- **Decomposable approximations for potential only.**
  For a given form of the potential $\tilde{v}_t[n] \approx \frac{\delta T_s[n]}{\delta n(\vec{r})}$, such that the corresponding expression for neither $\tilde{T}_s[n]$ nor $\tilde{v}_t^{nad}[n_A, n_B]$ is known, one can construct trivially the corresponding approximation for $\tilde{v}_t^{nad}[n_A, n_B]$.

$$v_t^{nad}[n_A, n_B] \approx \tilde{v}_t[n_A + n_B] - \tilde{v}_t[n_A] \tag{9.1.9}$$

  The field of applicability of such approximations is, however, limited. In the absence of the corresponding analytic expression for $\tilde{T}^{nad}[n_A, n_B]$, it is not possible to evaluate the total energy self-consistently with $\tilde{v}_t^{nad}[n_A, n_B]$ used in Eq. 9.1.3. It is sufficient, though, for obtaining the ground-state density of the embedded system as well as the embedded orbitals.
- **Non-decomposable approximations.**
  This is a bottom-up approach starting from an approximation for $v_t^{nad}[n_A, n_B]$ and than constructing the corresponding approximation for $T_s^{nad}[n_A, n_B]$:

$$v_t^{nad}[n_A, n_B] \approx \tilde{v}_t^{nad}[n_A, n_B] = \left.\frac{\delta \tilde{T}_s^{nad}[n, n_B]}{\delta n(\vec{r})}\right|_{n(\vec{r})=n_A(\vec{r})} \tag{9.1.10}$$

  In this approach, the parent approximation for neither $\tilde{T}_s[n]$ nor its functional derivative is constructed. The latter quantities are not directly needed in the FDET-based methods because the approximations are used only for the *differences* of such quantities. The NDSD approximation[6] for $T_s^{nad}[n_A, n_B]$ was constructed following this strategy.
- **Non-decomposable approximations for the potential only.**
  In principle, one can construct only $\tilde{v}_t[n_A, n_B]$ without constructing the corresponding approximation to $\tilde{T}_s^{nad}[n_A, n_B]$. This would make possible to obtain the embedded density and orbitals but not the total energy. To our knowledge, no such constructions, were reported in the literature.

Since the accuracy of the used approximation $\tilde{v}_t^{nad}[n_A, n_B]$ is of key importance in FDET-based methods, this issue was subject of our previous studies based on the comparisons between the electron density obtained using the analyzed approximation with the target electron density obtained if the approximation would be exact.[4,5,20] Such strategy to judge the adequacy of a given $\tilde{v}_t^{nad}[n_A, n_B]$ does not, however, involve the construction of the exact $v_t^{nad}(\vec{r})$. Moreover, the previous analyses focused on cases where the overlap between $n_A(\vec{r})$ and $n_B(\vec{r})$ is small because $n_A(\vec{r})$ and $n_B(\vec{r})$ were associated with different molecules in weak intermolecular complexes. This excluded such important case where $n_B(\vec{r})$ corresponds to fully occupied inner shell whereas $n_A(\vec{r})$ comprises contributions from the valence electrons and the potential $v_t^{nad}[n_A, n_B]$ is sufficiently repulsive to stop the valence electrons to collapse on the core region. The present work is intended to fill this gap. To this end, we use an artificial system for which the exact potential $v_t^{nad}(\vec{r})$ can be obtained analytically for particularly chosen $n_B(\vec{r})$.[22] The considered model system

comprises four electrons with spin-compensated density, it is spherically symmetric, and its exact Kohn-Sham potential reads:

$$v_{KS}(r) = -\frac{1}{r} \; . \tag{9.1.11}$$

Note that such a system does not correspond to any real atom. It is defined by its Kohn-Sham potential and not the external potential. Nevertheless, it can be used for the analysis of various density functionals. It is important to make the distinction between such an artificial system as the one considered here and the Be atom for which the Kohn-Sham potential comprises the nuclear attraction term $-4/r$, the repulsive Coulomb term, as well as the exchange-correlation component. It behaves as $-1/r$ only far from the nucleus.

For the considered system, the two doubly occupied Kohn-Sham orbitals are just hydrogenic functions: ϕ_{1s} and ϕ_{2s} and the ground-state electron density reads:

$$n_o(\vec{r}) = 2\left(\phi_{1s}^2 + \phi_{2s}^2\right) \; , \tag{9.1.12}$$

Concerning the choice for $n_B(\vec{r})$, we limit the analysis to cases where $n_o(\vec{r}) - n_B(\vec{r})$: *i*) is non-negative, *ii*) integrates to 2, and *iii*) is spin-compensated. These are necessary conditions that the density $n_o(\vec{r}) - n_B(\vec{r})$ can be obtained from the ground-state wavefunction for some potential $v_s(\vec{r})$ (Chapter 12 deals with the issue of the admissibility of the frozen density in more detail.) The potential $v_s(\vec{r})$ can be constructed by inverting analytically the Kohn-Sham equation associated with the density $n_o(\vec{r}) - n_B(\vec{r})$.[22]

$$\left[-\frac{1}{2}\nabla^2 + v_s(\vec{r})\right]\varphi = \epsilon\varphi \tag{9.1.13}$$

In the above equation $v_s(r)$ is such potential, for which the lowest-energy solution φ is such that $2|\varphi|^2 = n_o - n_B$. This potential reads thus:

$$v_s(\vec{r}) = \frac{1}{2}\frac{\nabla^2\sqrt{n_o(\vec{r}) - n_B(\vec{r})}}{\sqrt{n_o(\vec{r}) - n_B(\vec{r})}} + constant \; , \tag{9.1.14}$$

where the constant can be chosen such that the potential goes to 0 when $r \to \infty$.

Comparing Eqs. 9.1.3 and 9.1.13 provides a link between the potential $v_s(r)$ which can be obtained analytically and $v_t^{nad}[n_A, n_B](r)$ - the quantity of crucial interest in this study. To lead to the same density, the effective potential in Eq. 9.1.3 and $v_s(\vec{r})$ must be equal (up to a constant). From that it follows that, up to a constant,

$$v_t^{nad}(r) = v_s(r) + \frac{1}{r} \; . \tag{9.1.15}$$

The above analytic construction of $v_t^{nad}(\vec{r})$ can be made for any density $n_o(\vec{r}) - n_B(\vec{r})$ comprising two spin-compensated electrons and is not restricted to the case considered here (spherical symmetry and $\int n_B(\vec{r})d\vec{r} = 2$). Note also that the construction of the external potential $v_{ext}(\vec{r})$ in a real, i.e., interacting system

with the same ground state density given in Eq. 9.1.12 is not involved in the above analytical construction of the exact $v_t^{nad}(r)$. The choices for $n_B(\vec{r})$ in the above system considered in this work, are made in view of practical numerical simulations. If $n_B(\vec{r})$ is chosen to be electron density of the core electrons, the potential $v_t^{nad}(r)$ stops the density $n_A(\vec{r})$ derived from Eq. 9.1.3 from collapsing into the core. Such cases have been reported[6,23] for simulations using instead of the exact $v_t^{nad}(r)$ some approximations to the functional $v_t^{nad}[n_A, n_B]$. For more properties of the exact potential $v_t^{nad}[n_A, n_B](r)$ in the considered model system, see Ref.[22] The considered system, provides a simple illustration for the role of the potential $v_t^{nad}[n_A, n_B]$ in preventing such a collapse. If the electron density of the $1s$ shell is chosen as n_B (i.e., $n_B(\vec{r}) = 2\varphi_{1s}^2$), neglecting $v_t^{nad}[n_A, n_B]$ in Eq. 9.1.3 leads to wrong total electron density: $\tilde{n}_o(\vec{r}) = 2\left(\varphi_{1s}^2 + \varphi_{1s}^2\right) \neq n_o(\vec{r}) = 2\left(\varphi_{1s}^2 + \varphi_{2s}^2\right)$. One way to stop the collapse into the core is to use the exact pseudopotential as prescribed by Phillips-Kleinman[24] expressed with the projector operators. But such an operator is not a local potential and would require other than density descriptors for the environment. In our previous work, the local potential stopping such a collapse into the core was constructed and analyzed .[22] The present work, focuses on such cases, but extends the analysis by: *i*) obtaining numerically the lowest-energy embedded orbital derived from numerical solution of Eq. 9.1.3, *ii*) obtaining numerical solutions of an approximated version of Eq. 9.1.3 in which instead of the exact potential $v_t^{nad}(r)$ its approximated counterpart - $\tilde{v}_t^{nad}[n_A, n_B]$ - is used. The following approximations of $\tilde{v}_t^{nad}[n_A, n_B]$ are considered in the present work:

i) $\tilde{v}_t^{nad(W)}[n_A, n_B]$ obtained from Eq. 9.1.8 and the von Weizsäcker functional for $T_s[n]$[25],
ii) $\tilde{v}_t^{nad(TF)}[n_A, n_B]$ obtained from Eq. 9.1.8 and the Thomas-Fermi functional for $T_s[n]$,[26,27]
iii) $\tilde{v}_t^{nad(TFW)}[n_A, n_B]$ obtained from Eq. 9.1.8 and the sum of the Thomas-Fermi and the von Weizsäcker functionals for $T_s[n]$,
iv) $\tilde{v}_t^{nad(GEA2)}[n_A, n_B]$ obtained from Eq. 9.1.8 and the second-order gradient-expansion functional for $T_s[n]$,[28]
v) $\tilde{v}_t^{nad(CW)}[n_A, n_B]$ obtained from Eq. 9.1.9 and the Chai and Weeks approximation for $\frac{\delta T_s[n]}{\delta n}$.[29] Note that there exist no corresponding functional for $T_s[n]$ in this case.

Each among the considered approximats for the potential $\tilde{v}_t^{nad}[n_A, n_B]$ reflects some exact properties and does not involve any fitting to experimental data. Both the Thomas-Fermi- and the von Weizsäcker functionals are frequently considered to be possible starting points for construction of approximations to $T_s[n]$. The former one yields the exact $T_s[n]$ for uniform electron gas $n(\vec{r})$ =const, whereas the latter is exact of one-electron- or spin-compensated two electron systems, leads to rather erratic results.[4,20] Our previous numerical studies on the accuracy of various $\tilde{v}_t^{nad}[n_A, n_B]$ for cases where the overlap between $n_A(\vec{r})$ and $n_B(\vec{r})$ is small showed

that the Thomas-Fermi functional leads to a useful approximation for the potential $v_t^{nad}[n_A, n_B]$.[4,5,20,30] The von Weizsäcker functional leads, however, to the optimal density which is frequently qualitatively wrong.[20] Moreover, the addition of the second-order term leads frequently to worse $v_t^{nad}[n_A, n_B]$ than that derived from the Thomas-Fermi functional.[4,20]

The $\tilde{v}_t^{nad(TFW)}[n_A, n_B]$ approximation was considered in the present work in view of the fact that the presence of the full von Weizsäcker component (not divided by 9 as it is in gradient expansion) is indispensable to satisfy one of the exact conditions for $v_t^{nad}[n_A, n_B]$[6] (given also in Eq. 9.2.18 here). The full von Weizsäcker term is also a key ingredient for a family of approximations[31] for $T_s[n]$. The inclusion of the Chai-Weeks approximation for $\frac{\delta T_s[n]}{\delta n}$ in the present analysis is motivated by its feature to describe correctly the density response of the atomic electron density.

9.2. Numerical Results and Discussion

The numerical solutions of Eq. 9.1.3 using either the exact potential $v_t^{nad}(r)$ or its approximate counterparts, were obtained using the solver of one-dimensional Schrödinger equation[32] implemented into Mathematica.[33] We consider two choices for $n_B(\vec{r})$ such that it is "almost" equal to $2\varphi_{1s}^2$ and that $n_o(\vec{r}) - n_B(\vec{r})$ is non-negative. A small difference between $2\varphi_{1s}^2$ and the considered $n_B(\vec{r})$ assures that $v_t^{nad}(r)$ is continuous. As shown in our previous work,[22] the potential changes smoothly with changing the amount of the admixture provided it is small. The following two choices for $n_B(\vec{r})$ are considered:

- $n_B(\vec{r}) \approx 2\varphi_{1s}^2$ with "dumped valence density" admixture,

$$n_B(r) = \frac{1}{C}\left(\varphi_{1s}^2 + \varphi_{2s}^2 \cdot e^{-10r}\right) \tag{9.2.16}$$

  and where $1/C$ is the normalization factor.

- $n_B(\vec{r}) \approx 2\varphi_{1s}^2$ with "mixed core/valence" admixture,

$$n_B(r) = 2\left((1-w)\varphi_{1s}^2 + w\varphi_{2s}^2\right) , \tag{9.2.17}$$

  with $w = 0.001$.

  Eq. 9.2.17 choice for $n_B(\vec{r})$ was used in the analytical reconstruction of $v_t^{nad}(\vec{r})$ for the same model system[22] and is considered here for the sake of completeness and for comparisons.

The two above choices for $n_B(\vec{r})$ assure that $n_o(\vec{r}) - n_B(\vec{r})$ is N-representable. To obtain the density $n_o(\vec{r}) - n_B(\vec{r})$ as the lowest-energy solution of Eq. 9.1.3, this density must be non-interacting pure-state v-representable.[1,19]

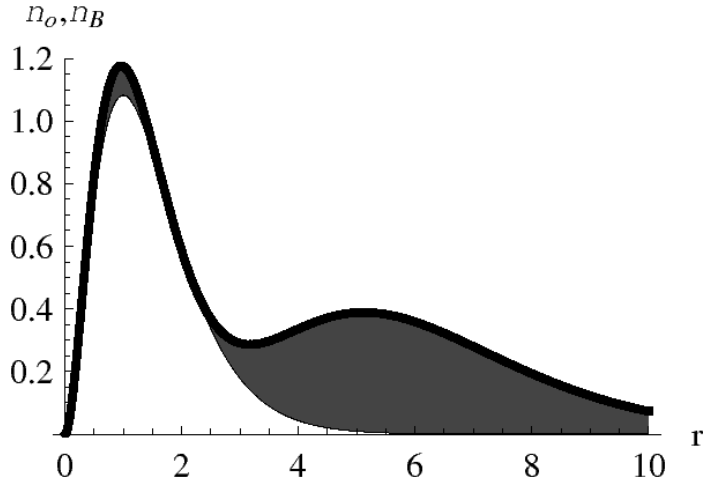

Fig. 9.2.1. Partitioning the total ground-state electron radial density $4\pi r^2 n_o(\vec{r})$ in the model system. The white area represents the frozen radial density $4\pi r^2 n_B(\vec{r})$ and the shaded area represents the radial density $4\pi r^2 \left(n_o(\vec{r}) - n_B(\vec{r})\right)$. Only the densities obtained with the Eq. 9.2.16 are shown because the alternative partitioning (Eq. 9.2.17) leads to densities indistinguishable on the scale of the picture.

9.2.1. *Eq. 9.1.3 with the exact potential* $v_t^{nad}(\vec{r})$

9.2.1.1. *The potential* $v_t^{nad}(\vec{r})$

The total effective potential in a system of non-interacting electrons, which generates $n_o(\vec{r}) - n_B(\vec{r})$ as its ground-state density comprises the $-1/r$ and $v_t^{nad}(\vec{r})$ components. Since $-1/r$ diverges at $r = 0$ and is known, only the $v_t^{nad}(\vec{r})$ is shown on the figures in this section. Figure 9.2.2 shows the reconstructed potential $v_t^{nad}(\vec{r})$ for the two considered choices for $n_B(\vec{r})$. The potential $v_t^{nad}(\vec{r})$ varies rapidly in both cases. At $r = 2$, i.e., where the target radial density has minimum in both considered cases, the potential has a spike. For $r = 2$, $v_t^{nad} = 204.82$ and $v_t^{nad} = 115.714$ for the Eq. 9.2.16 and Eq. 9.2.17 case, respectively. The presence of such a spike reflects the exact condition for $v_t^{nad}[n_A, n_B]$:[6]

$$v_t^{nad}[n_A, n_B]\big|_{n_A \longrightarrow 0, \int n_B(\vec{r})d\vec{r}=2} = \frac{1}{8}\frac{|\nabla n_B|^2}{n_B^2} - \frac{1}{4}\frac{\nabla^2 n_B}{n_B} \tag{9.2.18}$$

At these conditions, the exact potential $v_t^{nad}[n_A, n_B]$ is given by the functional derivative of the von Weizsäcker functional evaluated at the density n_B. We notice that the constraint $\int n_B(\vec{r})d\vec{r} = 2$ applies everywhere in the considered partitioning. The limit, $n_A \longrightarrow 0$ occurs, however, in three regions: at $r = 0$, 2, or ∞. At $r = 2$, $n_A(\vec{r})/n_B(\vec{r}) \to 0$ for either choices for $n_B(\vec{r})$. As a consequence of principally exponential behavior of $n_B(\vec{r})$, Eq. 9.2.18 leads to $v_t^{nad}[n_A, n_B]$, which is strongly positive at $r = 2$, for either choices of $n_B(\vec{r})$. At $r = 0$, however, the two choices for $n_B(\vec{r})$ lead to qualitatively different behavior of $v_t^{nad}[n_A, n_B]$. With the Eq. 9.2.16

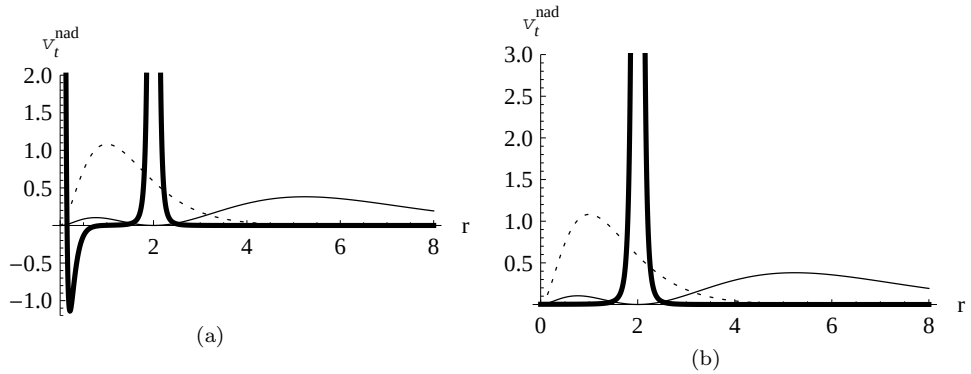

Fig. 9.2.2. The exact $v_t^{nad}(\vec{r})$ (thick lines): a) $n_B(\vec{r})$ given in Eq. 9.2.16, (b) $n_B(\vec{r})$ given in Eq. 9.2.17. The frozen radial density $4\pi r^2 n_B(\vec{r})$ (dotted line) and the target density $4\pi r^2 \left(n_o(\vec{r}) - n_B(\vec{r})\right)$ (solid line) also shown.

choice for $n_B(\vec{r})$, $n_A(\vec{r})/n_B(\vec{r}) \to 0.0007$ at $r \to 0$ leading to a spike at $r = 0$ for similar reasons as at $r = 2$. With the Eq. 9.2.17 choice for $n_B(\vec{r})$, $n_A(\vec{r})/n_B(\vec{r}) \to 0.125$ at $r \to 0$.

It is worthwhile to underline the the fact that, the potential $v_t^{nad}(\vec{r})$ is not the same in the case of $n_B(\vec{r})$ chosen as in either Eq. 9.2.16 or 9.2.17 although the target densities are very similar in both cases (indistinguishable on the scale used in Figure 9.2.1).

9.2.1.2. *Embedded orbital and embedded density*

Figure 9.2.3 shows the radial density obtained from the ground-state solution of Eq. 9.1.3 for $n_B(\vec{r})$ given in Eq. 9.2.16 and the exact potential $v_t^{nad}(\vec{r})$ given in Eqs. 9.1.14 and 9.1.15. The density $n_A(r)$, which is derived from numerical solution of Eq. 9.1.3, matches perfectly the target density $n_o(r) - n_B(r)$ which is obtained analytically.

The minimum of the radial density $4\pi r^2 \left(n_o(\vec{r}) - n_B(\vec{r})\right)$ at $r = 2$ is not zero ($n_o(2) - n_B(2) = 0.0003310$ for $n_B(r)$ given in Eq. 9.2.16). It can be made infinitely small with the exponential dumping factor in Eq. 9.2.16. This value is very accurately reproduced by the numerical solver of Eq. 9.1.3 for the exact potential ($n_A(2) = 0.0003317$). For $n_B(\vec{r})$ chosen as in Eq. 9.2.17, the behavior of the embedded density at $r = 2$ is very similar to the previously analyzed one. The radial density almost reaches zero for the chosen $w = 0.001$ and can be might infinitely small by decreasing w which correspond to the increase of the hight of the maximum in $v_t^{nad}(r)$.[22] The corresponding numerical values are: $n_o(2) - n_B(2) = 0.0005861$ and $n_A(2) = 0.0005864$. This result shows robustness of the used numerical procedure to solve Eq. 9.1.3 (see also the discussion of the overlaps in the subsequent parts of the present work).

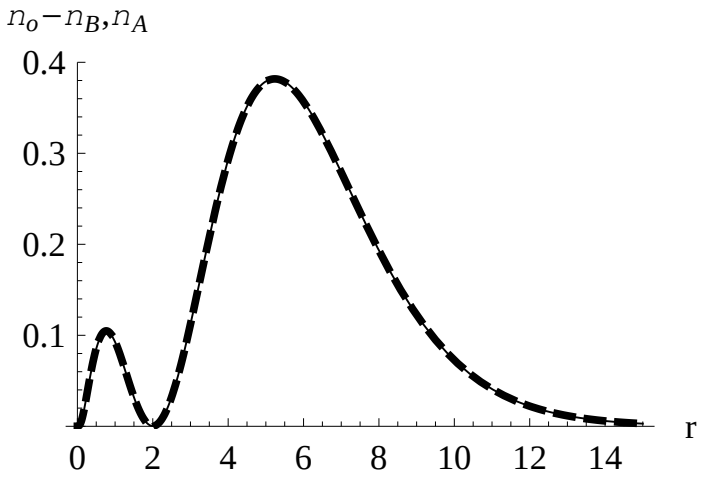

Fig. 9.2.3. Radial density $4\pi r^2 n_A(\vec{r})$ obtained from Eq. 9.1.3 with the exact $v_t(\vec{r})$ (solid line) and the target radial electron density $4\pi r^2 \left(n_o(\vec{r}) - n_B(\vec{r})\right)$ (dashed line). Only the densities obtained with the Eq. 9.2.16 are shown. The alternative partitioning (Eq. 9.2.17) leads to densities indistinguishable on the scale of the picture.

The ground-state embedded orbitals obtained from Eq. 9.1.3 for the two considered choices for $n_B(\vec{r})$ are shown on Figure 9.2.4. In each case, the orbital is node-less with a maximum at about $r = 5$, a minimum at $r = 2$, and the secondary maximum near the nucleus r. The embedded orbital closely orbitals resembles $|\varphi_{2s}|$. The switch of the sign from negative to positive at $r = 2$ is the consequence of the barrier in $v_t^{nad}(\vec{r})$ which makes the embedded orbital node-less. Most of the electron density is localized in the valence shell, i.e., at $r > 2$.

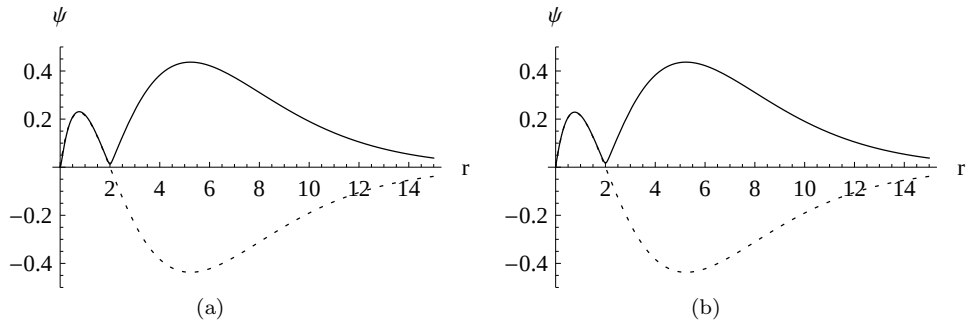

Fig. 9.2.4. The radial orbital obtained from Eq. 9.1.3 with the exact $v_t(r)$: (a) $4\pi r^2 n_B(\vec{r})$ given in Eq. 9.2.16 (b) $4\pi r^2 n_B(\vec{r})$ given in Eq. 9.2.17. The radial hydrogenic φ_{2s} function is shown for comparison (dotted line).

It is worthwhile to underline that the considered choices for $n_B(\vec{r})$ do not cor-

respond to freezing the density $2\varphi_{1s}^2$ because of the small admixture of the valence density in $n_B(\vec{r})$. Our previous analyses of the same system[22] show that $v_t^{nad}(r)$ changes smoothly with decreasing amount of the admixture, i.e., if $n_B(\vec{r})$ approaches $2\varphi_{1s}^2$. As the consequence, the embedded wavefunction obtained from Eq. 9.1.3 does not approach φ_{2s} but rather $|\varphi_{2s}|$ as $n_B(\vec{r}) \to 2\varphi_{1s}^2$ (see Figure 9.2.4). The embedded wavefunction cannot be, therefore, orthogonal to the orbital used to construct $n_B(\vec{r})$. This behavior of the embedded wavefunction illustrates the relation between the orbital-free embedding potential given in Eq. 9.1.1 and the exact pseudopotential as defined by Phillips and Kleinman[24] if the core orbitals would be chosen to be frozen. The exact Phillips-Kleinman pseudopotential and the orbital-free effective embedding potential achieve the same target density in a different manner. In the former case, the target density corresponds to the ground-state of some system for which the external potential was modified. In the latter one, the target density corresponds to the excited state of the non-modified system. The excited state becomes a ground state owing to projecting out the ground-state solution which involves non-local operators. In the Phillips-Kleinman pseudopotential case, the exact valence orbital has a node as it must be orthogonal to φ_{1s}. The lowest-energy embedded orbital approaches a node-less function if $n_B(\vec{r}) \to 2\varphi_{1s}^2$ and cannot be, therefore, orthogonal to φ_{1s}.

9.2.1.3. *The non-additive kinetic energy*

In the considered systems, the numerical value of $T_s^{nad}[n_o - n_B, n_B] = T_s[n_o] - T_s[n_o - n_B] - T_s[n_B]$ is available in a form of an analytic expression. The kinetic energy $T_s[n_o]$ is obtained as the expectation value of the kinetic operator calculated for the non-interacting wavefunction constructed from two known doubly occupied Kohn-Sham orbitals. For $T_s[n_o - n_B]$ and $T_s[n_B]$, the situation is even simpler as $n_o - n_B$ and n_B represent doubly-occupied one-orbital systems. $T_s^{nad}[n_o - n_B, n_B]$ is non-zero for both considered choices for $n_B(\vec{r})$. $T_s^{nad}[n_o - n_B, n_B] = 0.00629883$ and $T_s^{nad}[n_o - n_B, n_B] = 0.013866$, for the Eq. 9.2.16 and Eq. 9.2.17 cases, respectively. Interestingly, the local behavior of the radial integrand $t_s^{nad}[n_o - n_B, n_B](r) = t_s[n_o - n_B](r) - t_s[n_o](r) - t_s[n_B](r)$ used to obtain $T_s^{nad}[n_o - n_B, n_B] = \int_0^\infty t_s^{nad}[n_o - n_B, n_B](r)dr$ behaves quite differently in both considered cases (see Figure 9.2.5).

For the Eq. 9.2.17 case, also $t_s^{nad}(r)$ is non-negative (see Figure 9.2.5), in line with a more general result that $t_s^{nad}[n_A, n_B]$ is non-negative for the partitioning of the total electron density based on mixing of orbital densities in any four-electron system.[34]

In the Eq. 9.2.16 case, although $T_s^{nad}[n_A, n_B]$ is positive, $t^{nad}(r)$ changes sign from negative to positive at about $r = 0.34$. It is worthwhile to notice that neither the Thomas-Fermi- nor the von Weizsäcker approximation to $T_s[n]$ could yield such a behavior because the former leads to non-negative, whereas the latter one to non-positive $t^{nad}(r)$.

It is worthwhile to underline that, although the integrand $t^{nad}(r)$ can be inter-

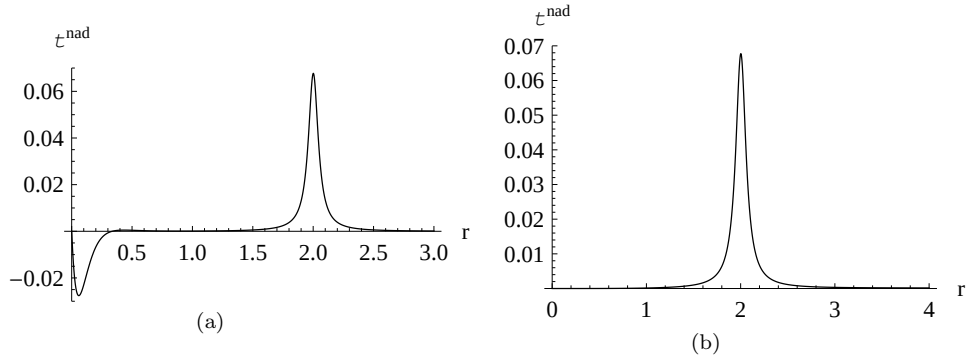

Fig. 9.2.5. The radial integrand $t_s^{nad}(r)$ in $T_s^{nad}[n_o - n_B, n_B] = \int_0^\infty t_s^{nad}[n_o - n_B, n_B](r)dr$ for two choices for n_B: (a) $n_B(\vec{r})$ given in Eq. 9.2.16, (b) $n_B(\vec{r})$ given in Eq. 9.2.17.

preted as the radial density of the non-additive kinetic energy, the latter quantity is not uniquely defined because any function integrating to zero will not affect T_s^{nad}.

9.2.2. *Eq. 9.1.3 with the approximated potentials* $\tilde{v}_t^{nad}[n_A, n_B]$

The considered approximated potentials $\tilde{v}_t^{nad}[n_A, n_B]$ are shown in Figures 9.2.6 and 9.2.7. None of them reproduces adequately the whole shape of $v_t^{nad}(\vec{r})$.

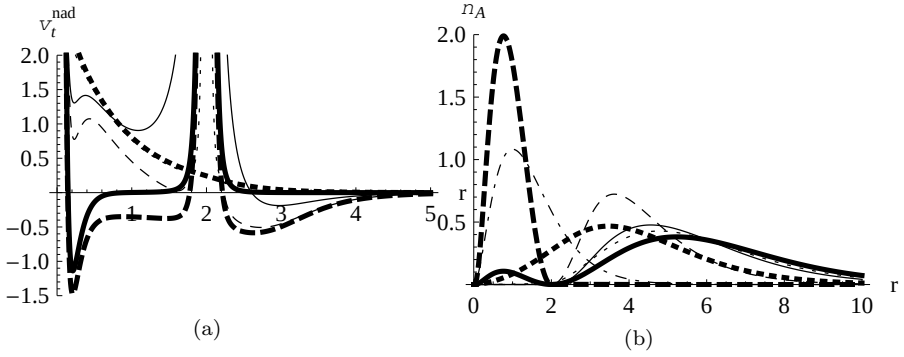

Fig. 9.2.6. The exact potential $v_t^{nad}(\vec{r})$ (bold), its approximated counterparts: $\tilde{v}_t^{nad(TF)}[n_A, n_B]$ (bold dotted), $\tilde{v}_t^{nad(W)}[n_A, n_B]$ (bold dashed), $\tilde{v}_t^{nad(GEA2)}[n_A, n_B]$ (dotted), $\tilde{v}_t^{nad(TFW)}[n_A, n_B]$ (dashed), and $\tilde{v}_t^{nad(CW)}[n_A, n_B]$ (solid), and the corresponding ground-state densities of the embedded system obtained for the Eq. 9.2.16 choice for $n_B(\vec{r})$: (a) potentials $v_t^{nad}(\vec{r})$ and $\tilde{v}_t^{nad}[n_A, n_B]$, (b) embedded radial densities $4\pi r^2 n_A(\vec{r})$ and $4\pi r^2 \tilde{n}_A(\vec{r})$). The dot-dashed line is the density obtained for $\tilde{v}_t^{nad}[n_A, n_B] = 0$.

The potential $\tilde{v}_t^{nad(TF)}[n_A, n_B]$ decays monotonically differing qualitatively from the exact potential. In particular, the barrier at $r = 2$ occurring in both choices for $n_B(\vec{r})$ is not reproduced. In the Eq. 9.2.16 case, instead of a narrow spike in $v_t^{nad}(r)$

at $\to 0$, $\tilde{v}_t^{TF}[n_A, n_B]$ is significantly lower and wider. Moreover, $\tilde{v}_t^{nad(TF)}[n_A, n_B]$ is very similar for both choices for $n_B(\vec{r})$ (either Eqs. 9.2.16 or 9.2.17, whereas the exact potential $v_t^{nad}(r)$ at $r \to 0$ differs qualitatively in these two cases.

As far as the qualitative behavior of the exact potential is concerned, $\tilde{v}_t^{nad(W)}[n_A, n_B]$ seems to be much better than $\tilde{v}_t^{TF}[n_A, n_B]$. Up to about $r = 2$, $\tilde{v}_t^{nad(W)}[n_A, n_B]$ and the exact potential are just shifted by almost a constant: from 0.333463 at $r \to 0$ to 0.490454 at $r = 2$ in the Eq. 9.2.16 case. The corresponding shifts for $n_B(\vec{r})$ chosen as in Eq. 9.2.17 are 0.333335 and 0.49045. For the Eq. 9.2.16 choice for $n_B(\vec{r})$, the maximum of the exact potential at $r = 2$ amounts to 204.82, whereas the corresponding value for $\tilde{v}_t^{nad(W)}[n_A, n_B]$ is 204.329 (not shown in the figures). In the Eq. 9.2.17 case, the corresponding hights of the barrier are: $v_t^{nad}(2)$ =115.714 and $\tilde{v}_t^{nad(W=}[n_A, n_B](2) = 115.223$. Beyond $r = 2$, the magnitude of the shift between $\tilde{v}_t^{nad(W)}[n_A, n_B]$ and $v_t^{nad}(r)$ diminishes to vanish at large r. As the result, $\tilde{v}_t^{nad(W)}[n_A, n_B]$ is too negative for $2 < r < 4$.

The shape of $\tilde{v}_t^{nad(GEA2)}[n_A, n_B]$ reflects the strengths and weaknesses of its $\tilde{v}_t^{nad(TF)}[n_A, n_B]$ and $\tilde{v}_t^{nad(W)}[n_A, n_B]$ components (see Figures 9.2.6 and 9.2.7). On the scale of the pictures, $\tilde{v}_t^{nad(GEA2)}[n_A, n_B]$ is indistinguishable from the exact potential for $r > 2.2$. The barrier at $r = 2$ is about one order of magnitude too low due to the 1/9 factor in front of the von Weizsäcker contribution to $\tilde{v}_t^{nad(GEA2)}[n_A, n_B]$. Compared to $\tilde{v}_t^{nad(W)}[n_A, n_B]$, the reduction of its contribution (negative) and the addition of the Thomas-Fermi component eliminates almost perfectly the artificial negativity of $\tilde{v}_t^{nad(W)}[n_A, n_B]$ at $r > 2$. At $r < 1.7$, the $\tilde{v}_t^{nad(TF)}[n_A, n_B]$ component of this approximated potential dominates. As a result, $\tilde{v}_t^{nad(TF)}[n_A, n_B]$ and $\tilde{v}_t^{nad(GEA2)}[n_A, n_B]$ are practically the same at small r. The $\tilde{v}_t^{nad(TFW)}[n_A, n_B]$ potential reproduces adequately the barrier at small r but the weaknesses of its $\tilde{v}_t^{nad(W)}[n_A, n_B]$ component become apparent beyond $r = 2$.

The potential $\tilde{v}_t^{nad(CW)}[n_A, n_B]$ reproduces the barrier at $r = 2$ which is, however, too wide and too low. Moreover, it is too negative at $r > 2.5$. The width of the barrier at $r = 2$ is significantly overestimated. At small r, deficiencies of the Thomas-Fermi component of $\tilde{v}_t^{nad(CW)}[n_A, n_B]$ become apparent.

Using the exact potential $v_t^{nad}(\vec{r})$ in Eq. 9.1.3 leads to the density $n_A(\vec{r})$ which equals to the target density $n_o(\vec{r}) - n_B(\vec{r})$. In all examples considered in the present work, the target density is given analytically as $n_o(\vec{r}) - n_B(\vec{r})$. Replacing $v_t^{nad}(\vec{r})$ by some approximation $\tilde{v}_t^{nad}[n_A, n_B]$ leads to the embedded orbital and the embedded electron density denoted by $\tilde{n}_A(\vec{r})$, which might differ from $n_o(\vec{r}) - n_B(\vec{r})$. Similarly, the lowest energy embedded orbital in such a case might differ from $\sqrt{(n_o(\vec{r}) - n_B(\vec{r}))/2}$. Figures 9.2.6 and 9.2.7 show the densities ($\tilde{n}_A$) obtained using the considered approximations $\tilde{v}_t^{nad}[n_A, n_B]$.

In practical calculations using Eq. 9.1.3, approximations are needed not directly for $T_s[n]$ but for $T_s^{nad}[n_A, n_B]$ (in the evaluation of energy) and for $v_t^{nad}[n_A, n_B]$ (in the evaluation of embedded orbitals). To discuss the quality of these quantities in the approximated case, Tables 9.1 and 9.2 collect the numerical vales of: $T_s[n_o]$,

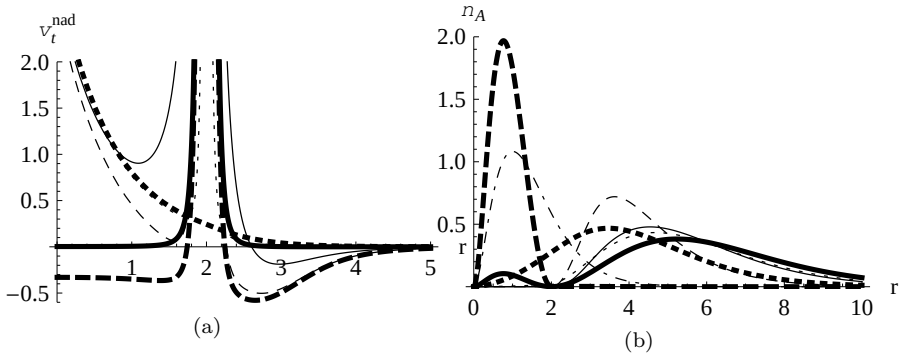

Fig. 9.2.7. The exact potential $v_t^{nad}(\vec{r})$ (bold), its approximated counterparts: $\tilde{v}_t^{nad(TF)}[n_A, n_B]$ (bold dotted), $\tilde{v}_t^{nad(W)}[n_A, n_B]$ (bold dashed), $\tilde{v}_t^{nad(GEA2)}[n_A, n_B]$ (dotted), $\tilde{v}_t^{nad(TFW)}[n_A, n_B]$ (dashed), and $\tilde{v}_t^{nad(CW)}[n_A, n_B]$ (solid), and the corresponding ground-state densities of the embedded system obtained for the Eq. 9.2.17 choice for $n_B(\vec{r})$: (a) potentials $v_t^{nad}(\vec{r})$ and $\tilde{v}_t^{nad}[n_A, n_B]$, (b) embedded radial densities $4\pi r^2 n_A(\vec{r})$ and $4\pi r^2 \tilde{n}_A(\vec{r})$). The dot-dashed line is the density obtained for $\tilde{v}_t^{nad}[n_A, n_B] = 0$.

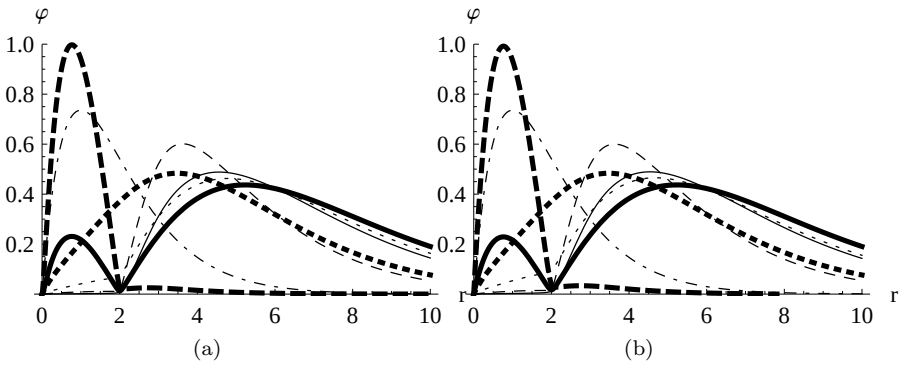

Fig. 9.2.8. The radial ground-state wavefunction obtained from Eq. 9.1.3 with the exact potential $v_t^{nad}(\vec{r})$ (bold), and its approximated counterparts: $\tilde{v}_t^{nad(TF)}[n_A, n_B]$ (bold dotted), $\tilde{v}_t^{nad(W)}[n_A, n_B]$ (bold dashed), $\tilde{v}_t^{nad(GEA2)}[n_A, n_B]$ (dotted), $\tilde{v}_t^{nad(TFW)}[n_A, n_B]$ (dashed), and $\tilde{v}_t^{nad(CW)}[n_A, n_B]$ (solid). The dot-dashed line is the density obtained for $\tilde{v}_t^{nad}[n_A, n_B] = 0$. (a) $n_B(\vec{r})$ given in Eq. 9.2.16, (b) $n_B(\vec{r})$ given in Eq. 9.2.17

$T_s^{nad}[n_o - n_B, n_B]$, and the overlap between the analytically obtained exact wavefunction:

$$\varphi_{exact}(\vec{r}) = \sqrt{\left(n_o(\vec{r}) - n_B(\vec{r})\right)/2} \tag{9.2.19}$$

and the wavefunction obtained from Eq. 9.1.3: either that with the exact potential (φ) or with one of the considered approximations ($\tilde{\varphi}$). The corresponding exact quantities available in the considered case are also given for comparison.

Table 9.1. Exact and approximate quantities calculated for $n_B(\vec{r})$ given in Eq. 9.2.16.

Approximation	$\tilde{T}_s[n_o]$	$\tilde{T}_s^{nad}[n_o - n_B, n_B]$	$\langle\varphi_{exact}\|\tilde{\varphi}\rangle$
none	0	0	0.375866
W	1.07179	-0.171912	0.245701
TF	1.10746	0.127427	0.864161
GEA2	1.22655	0.108325	0.974925
TFW	2.17925	-0.0444851	0.846614
CW	-	-	0.960765
exact	1.25	0.00629883	0.999992

Table 9.2. Exact and approximate quantities calculated for $n_B(\vec{r})$ given in Eq. 9.2.16.

Approximation	$\tilde{T}_s[n_o]$	$\tilde{T}_s^{nad}[n_o - n_B, n_B]$	$\langle\varphi_{exact}\|\tilde{\varphi}\rangle$
none	0	0	0.37779
W	1.07179	-0.164344	0.254705
TF	1.10746	0.130186	0.863955
GEA2	1.22655	0.111925	0.972546
TFW	2.17925	-0.0341583	0.848841
CW	-	-	0.9597
exact	1.25	0.013866	0.99999

Depending on which quantity is used as the accuracy criterion, the order of errors due to the approximations is different. For $T_s[n_o]$, the error in its approximate counterparts decreases in following the order:

$$none > TFW > W > TF > GEA2.$$

For $\tilde{T}_s^{nad}[n_o - n_B, n_B]$, the errors are ordered differently:

$$none > W > TF > GEA2 > TFW.$$

Finally, the errors in the embedded orbital (and the embedded density) measured as the deviations of $\langle\varphi_{exact}|\tilde{\varphi}\rangle$ from one, which indicate errors in $\tilde{v}_t^{nad}[n_A, n_B]$, are ordered in yet another way:

$$W > none > TFW > TF > CW > GEA2$$

The flaws of $\tilde{v}_t^{nad(W)}[n_o - n_B, n_B]$ result in the smallest overlap between the exact- and approximated embedded wavefunctions. It is even smaller (about 0.25) than if this component of the embedding potential is neglected (about 0.38)! $\tilde{v}_t^{nad(TF)}[n_o - n_B, n_B]$ is significantly better as the overlap between the approximated- and exact embedded wavefunctions increases to about 0.86. The Thomas-Fermi approximation stops the embedded density to collapse into the core

but does it only partially (see Figure 9.2.8). $\tilde{v}_t^{nad(GEA2)}[n_o - n_B, n_B]$ is very efficiently blocking such a collapse into the core as the position of the maximum of the radial wavefunction is almost in the right place. As a result, the overlap with the exact orbital is close to 1. The deficiency of this approximation is most pronounced in the core region where the exact wavefunction still has a small secondary minimum whereas the GEA2 wave function is very small. This is probably the result of the Thomas-Fermi component of $\tilde{v}_t^{nad(GEA2)}[n_o - n_B, n_B]$.

The $\tilde{T}_s^{nad(CW)}[n_o - n_B, n_B]$ and $\tilde{T}_s^{nad(TFW)}[n_o - n_B, n_B]$ approximations lead to noticeable worse embedded wavefunction than $\tilde{T}_s^{nad(GEA2)}[n_o - n_B, n_B]$. These approximations lead, however, to significantly better embedded wavefunction then $\tilde{T}_s^{nad(TF)}[n_o - n_B, n_B]$. Basically the same conclusions concerning the quality of approximations can be drawn from the results for the Eq. 9.2.17 choice for $n_B(\vec{r})$ (see Table 9.2).

The superiority of the $\tilde{v}_t^{nad(GEA2)}[n_A, n_B]$ in preventing the collapse from valence into the core does not mean that this approximation is universally the best. The present work, concerns cases with a strong overlap between $n_A(\vec{r})$ and $n_B(\vec{r})$. Our previous studies for such pairs $n_A(\vec{r})$ and $n_B(\vec{r})$, which do not overlap significantly ,[11,20] show that $\tilde{v}_t^{nad(GEA2)}[n_A, n_B]$ leads to erratic results as far as the embedded density is concerned. This flaw of $\tilde{v}_t^{nad(GEA2)}[n_A, n_B]$ was recently reconfirmed by Gotz et al.[21] Cutting off smoothly this term, as it is made in the GGA97 approximation for $\tilde{v}_t^{nad(GEA2)}[n_A, n_B]$[30] largely expands the area of applicability of Eq. 9.1.3.[5]

9.3. Conclusions

The present work reports the complete application of one-electron equations for embedded orbitals in analytically solvable case. All the quantities related to the kinetic energy, which are approximated in practical calculations, i.e., *i*) the non-additive kinetic energy $T_s^{nad}[n_A, n_B]$ together with its radial distribution $t_s^{nad}[n_A, n_B](r)$, *ii*) the potential $\tilde{v}_t^{nad}(\vec{r})$, and *iii*) the embedded orbital and *iv*) the embedded density are obtained analytically. These quantities are compared with their approximated counterparts. Concerning the exact calculations, the orbital-free embedding potential was constructed following the same steps as in our previous work[22] in the same model system but for other choices for the frozen component $n_B(\vec{r})$. The present work complements the previous studies by obtaining numerically the embedded orbitals and embedded electron density from the Eq. 9.1.3 for either the exact or approximated non-additive kinetic energy potential. It is shown that, indeed, the lowest-energy solution of Eq. 9.1.3 with the *exact effective potential* leads to the target density even in the case where the target density is localized in the valence shell. In computational methods in common use, such a collapse of the density into the core is avoided by means of a non-local operator such as the Phillips-Kleinman pseudopotential. Here, it is shown that a local potential can be used for the same

purpose although the obtained orbital is quite different as it must yield the same electron density as that of the valence shell being still node-less. The radial distribution $t_s^{nad}[n_A, n_B]$ of the contributions to $T_s^{nad}[n_A, n_B]$) show that it can change sign in some cases. This indicates that the each of the two canonical approximations to $T_s[n]$ (Thomas-Fermi- and von Weizsäcker) might be entirely inadequate in some regions in space as the Thomas-Fermi approximations leads always to non-additive $t_s^{nad}[n_A, n_B]$ whereas the latter one leads to always non-positive $t_s^{nad}[n_A, n_B]$.

Concerning the approximate potentials, their capacity to prevent the valence density to collapse into the core varies strongly from one approximation to another. The local density approximation leads to a monotonically decreasing repulsive potential, which prevents the collapse only partially. The exact functional for a close-shell two electron system (the von Weizsäcker functional for $T_s[n]$ leads to the embedding potential, which is even worse than such in which the non-additive kinetic energy potential is completely neglected. As far as semi-local approximations for $T_s[n]$ are concerned, it is clearly demonstrated that improving the approximation for $T_s[n]$ does not necessarily lead to improvements in the quantities derived from such approximations - the potential $v_t^{nad}[n_A, n_B]$ in particular. This indicates that the quest for a good approximations for $v_t^{nad}[n_A, n_B]$ is governed by its own rules. The challenge of accurate approximations for the functional $T_s[n]$ and its functional derivative, i.e., quantities which are of key importance for OF-DFT methods overviewed in the present volume, is not necessarily directly related to the efforts in approximating $T_s^{nad}[n_A, n_B]$ and its functional derivative, which are key ingredients in the FDET-based methods.

The provided numerical examples provide also a good illustration for the highly non-local nature of the relation between the orbital-free embedding potential and embedded electron density. The three approximated potentials: $\tilde{v}_t^{nad(GEA2)}[n_A, n_B]$, $\tilde{v}_t^{nad(TFW)}[n_A, n_B]$, and $\tilde{v}_t^{nad(CW)}[n_A, n_B]$, although are quite different, lead to rather similar embedded electron densities. Among them $\tilde{v}_t^{nad(GEA2)}[n_A, n_B]$ is clearly the best one for the considered pairs n_A and n_B.

Concerning development of approximations for $\tilde{v}_t^{nad}[n_A, n_B]$, the present study indicates that the approximation should comprise the von Weizsäcker term in some regions of space (as it is made in the NDSD approximation for the non-additive kinetic energy[6]) although it can be scaled down as it is in the second order gradient expansion for $T_s[n]$. Its full inclusion in some regions in space, however, undesired.

Finally, we note that this work concerned properties of the bi-functional $T_s^{nad}[n_A, n_B]$ for a given n_B as in typical FDET-based computations (frozen n_B), the issue of approximating this bi-functional and its functional derivative by means of some explicit analytical expresions is also of key importance in fully variational calculations in which n_B is also subject to optimization. Such fully variational calculations are based on the subsystem formulation of DFT formulated by Senatore and Subbaswamy [35] and CortonaCortona1991. In practice, fully variational calculations can be performed using any implementation of FDET by means of the

"freeze-and-thaw" algorithm[11] involving iterative solutions of the KSCED equations for each interacting subsystem. We can expect, therefore, that errors of any approximation for $T_s^{nad}[n_A, n_B]$ considered in the present work would rather enhance than attenuate in fully variational calculations.

Acknowledgments

T.A.W. and A.S. acknowledge the support from the grants by Swiss National Research Foundation (Project 200020-134791) and ANR (Project 07-BLAN-0272), respectively.

References

1. T. A. Wesolowski and A. Warshel, *J. Phys. Chem.* **97**, 8050 (1993).
2. C. R. Jacob, J. Neugebauer, and L. Visscher, *J. Comput. Chem.* **29**, 1011 (2008).
3. J .W. Kaminski, S. Gusarov, A. Kovalenko, and T. A. Wesolowski, *J. Phys. Chem. A* **114**, 6082 (2010).
4. T. A. Wesolowski and J. Weber, *Int. J. Quantum Chem.* **61**, 303 (1997).
5. T. A. Wesolowski, *J. Chem. Phys.* **106**, 8516 (1997).
6. J. M. G. Lastra, J. W. Kaminski, and T. A. Wesolowski, *J. Chem. Phys.* **129**, 074107, 2008).
7. M. E. Casida and T. A. Wesolowski, *Int. J. Quantum Chem.* **96**, 577 (2004).
8. T. A. Wesolowski, *J. Am. Chem. Soc.* **126,** 11444 (2004).
9. T. A. Wesolowski, *Phys. Rev. A.* **77**, 012504 (2008).
10. K. Pernal and T. A. Wesolowski, *Int. J. Quant. Chem.* **109**, 2520 (2009).
11. T. A. Wesolowski and J. Weber, *Chem. Phys. Lett.* **248**, 71 (1996).
12. ADF2009 suite of programs Theoretical Chemistry Department, Vrije Universiteit, Amsterdam http://www.scm.com. 2009
13. W. Kohn and L. J. Sham, *Phys. Rev.* **140**, A1133, (1965).
14. M. Levy, *Proc. Natl. Acad. Sci. U.S.A.* **76**, 6062 (1979); see also: M. Levy, *Phys. Rev. A* **26**, 1200, (1982).
15. E. Lieb, *Int. J. Quant. Chem.* **24**, 243 (1983).
16. N. Govind, Y. A. Wang, and E. A. Carter, *J. Chem. Phys.* **110**, 7677 (1999).
17. A. S. P. Gomes, C. R. Jacob, and L. Visscher, *Phys. Chem. Chem. Phys.* **10**, 5353 (2008).
18. M. Hodak, W. Lu, and J. Bernholc, *J. Chem. Phys.* **128**, 014101, (2008).
19. T. A. Wesolowski. One-electron equations for embedded electron density: challenge for theory and practical payoffs in multi-level modelling of soft condensed matter. In ed. J. Leszczynski, *Computational Chemistry: Reviews of Current Trends*, vol. X, pp. 1–82. World Scientific, Singapore, (2006).
20. Y. A. Bernard, M. Dulak, J. W. Kaminski, and T. A. Wesolowski, *J. Phys. A-Math. Theor.* **41**, 055302, (2008).
21. A. W. Gotz, S. M. Beyhan, and L. Visscher, *J. Chem. Theor. & Comput.* **5**, 3161 (2009).
22. A. Savin and T. A. Wesolowski, *Prog. Theor. Chem. Phys.* **19**, 327 (2009).

23. C. R. Jacob, S. M. Beyhan, and L. Visscher, *J. Chem. Phys.* **126** , 234116, (2007).
24. J. Phillips and L. Kleinman, *Phys. Rev.* **116**, 287 (1959).
25. C. F. von Weizsäcker, *Z. Phys.* **96**, 431, (1935).
26. L. H. Thomas, *Proc. Cambridge Philos. Soc.* **23**, 542, (1927).
27. E. Fermi, *Z. Phys.* **48**, 73, (1928).
28. D. A. Kirzhnits, *Sov. Phys. JETP.* **5**, 64, (1957).
29. J. D. Chai and J. A. Weeks, *J. Phys. Chem. B* **108**, 6870 (2004).
30. T. A. Wesolowski, H. Chermette, and J. Weber, *J. Chem. Phys.* **105**, 9182 (1996).
31. P. K. Acharya, L. J. Bartolotti, S. B. Sears, and R. G. Parr, *Proc. Natl. Acad. USA.* **77**, 6978 (1980).
32. W. Lucha and F. Schoberl, *Intl. J. Mod. Phys. C.* **10**, 607 (1999).
33. S. Wolfram, *The Mathematica book.* 2003, fifth edition. ISBN 1-57955-022-3.
34. T. A. Wesolowski, *Mol. Phys.* **103**, 1165 (2005).
35. G. Senatore and K. R. Subbaswamy, *Phys. Rev. B* **34**, 5754 (1986).
36. P. Cortona, *Phys. Rev. B* **44**, 8454 (1991).